


ARTICLE

DOI: 10.1038/s41467-018-04528-7

OPEN

Interfacial photochemistry at the ocean surface is a global source of organic vapors and aerosols

Martin Brüggemann ^{1,2}, Nathalie Hayeck ¹ & Christian George ¹

The surface of the oceans acts as a global sink and source for trace gases and aerosol particles. Recent studies suggest that photochemical reactions at this air/water interface produce organic vapors, enhancing particle formation in the atmosphere. However, current model calculations neglect this abiotic source of reactive compounds and account only for biological emissions. Here we show that interfacial photochemistry serves as a major abiotic source of volatile organic compounds (VOCs) on a global scale, capable to compete with emissions from marine biology. Our results indicate global emissions of 23.2–91.9 TgC yr⁻¹ of organic vapors from the oceans into the marine atmosphere and a potential contribution to organic aerosol mass of more than 60% over the remote ocean. Moreover, we provide global distributions of VOC formation potentials, which can be used as simple tools for field studies to estimate photochemical VOC emissions depending on location and season.

¹Univ Lyon, Université Claude Bernard Lyon 1, CNRS, IRCELYON, F-69626 Villeurbanne, France. ²Present address: Leibniz Institute for Tropospheric Research (TROPOS), Permoserstr. 15, 04318 Leipzig, Germany. Correspondence and requests for materials should be addressed to C.G. (email: christian.george@ircelyon.univ-lyon1.fr)

Life on Earth is a constant and versatile source of surface-active compounds (i.e., surfactants) in the ambient environment. Biogenic surfactants are, therefore, omnipresent on surfaces exposed to the open atmosphere, ranging from lakes and rivers to cloud droplets, and aerosol particles¹. Nonetheless, the most prominent example of a surfactant-enriched surface is probably the ocean, covering more than 70% of Earth. Studies have shown that this air/water interface is almost ubiquitously covered by a thin film of amphiphilic compounds, which are enriched there with respect to the bulk water^{2–7}. Such sea surface microlayers (SMLs) were found to have significant effects on marine biogeochemical as well as climate related mechanisms by directly affecting processes such as exchange of trace gases (e.g., CO₂), heat, and aerosol particles³. In addition, recent field studies^{8,9} confirmed for the first time previous laboratory observations^{10–15} suggesting that irradiation of this air/water interface by sunlight produces organic vapors, known to enhance particle formation in the atmosphere. These emissions were attributed to purely photochemical reactions occurring in the SML. However, current model calculations neglect this abiotic source of reactive compounds and account only for organic vapors that are produced directly by biological processes^{16–20}.

Here, we combine for the first time results on the formation and presence of SMLs with observations of photochemical production of organic vapors from irradiation of surfactant-enriched air/water interfaces^{10–15}, to identify locations and time periods in which such photochemistry is of major importance for marine VOC levels. Moreover, we explore the global extent of such yet underestimated VOC emissions as well as their implications for organic aerosol (OA) mass in marine environments. Our estimations are based on a collection of photochemical VOC production parameters, surface UV irradiation, biological activity, and surface wind speeds. Using these variables, we estimate SML coverage of the oceans and VOC formation potentials from interfacial photochemistry on a 1° × 1° global grid. We infer potential OA mass contributions from photochemically produced VOCs using aerosol partitioning theory and a one-dimensional volatility basis set approach^{21–23}. As we demonstrate, accounting for abiotic photochemical VOC production closes current gaps in our understanding of atmospheric chemistry in remote regions and underlies the importance of the interplay between biology and chemistry for climatic processes. We infer global emissions of 32.5–129 Tg C yr⁻¹ (23.2–91.9 Tg C yr⁻¹) of organic vapors from the oceans into the marine atmosphere. Moreover, our results suggest a potential contribution to organic aerosol mass of more than 60% over the remote ocean. In addition, to support planning and design of future field studies with a focus on VOC emissions from interfacial photochemistry, we provide global distributions of VOC emission potentials as well as a small calculation tool based on Matlab, to estimate photochemical VOC emissions depending on location and season.

Results

Global sea surface microlayer coverage. Since VOC formation from interfacial photochemistry will only occur in the presence of surfactants, our starting point is the global SML coverage of the oceans. The exact spatial and temporal dynamics of these surface films are largely dependent on local biological and meteorological conditions. In particular, high wind speeds at the ocean's surface were shown to disturb the formation of such SMLs by breaking waves. The upper limit for the formation of SMLs was previously^{2,24} estimated to wind speeds of 8–10 m s⁻¹, however, recent field observations²⁵ suggest SML coverage even up to wind speeds of 13 m s⁻¹.

Following the approach of Wurl et al.², we use biological net productivity and mean surface wind speeds to derive global SML distributions. As shown in Fig. 1, the largest effects for different wind speed thresholds are especially observed for the Southern Ocean, North Pacific, and North Atlantic. Our results indicate that these regions are largely free of SMLs for a wind speed limit of 8 m s⁻¹ (Fig. 1a). In contrast, for a wind speed limit of 13 m s⁻¹ almost the entire surface of the oceans can be regarded as covered at least partially by SMLs (Fig. 1c). A transition state between these two extremes, previously² used to estimate the global presence of SMLs is shown in Fig. 1b.

Photochemical potential of the surface of the oceans. Assuming a linear relationship between photochemical VOC production and solar radiation as well as a logarithmic decay with decreasing surfactant concentrations^{10,11}, we can calculate a daily photochemical VOC emission potential μ_{photo} for the air/water interface of each grid cell:

$$\mu_{\text{photo}} = t_{\text{sun}} \cdot UV_{\text{a,b}} \cdot F_{\text{surfactant}} \cdot k_g \quad (1)$$

with the length of the day t_{sun} (in s), solar radiation $UV_{\text{a,b}}$ at the Earth's surface (280–400 nm, in mW cm⁻² day⁻¹), and a correction factor $F_{\text{surfactant}}$ to account for SML presence and surfactant

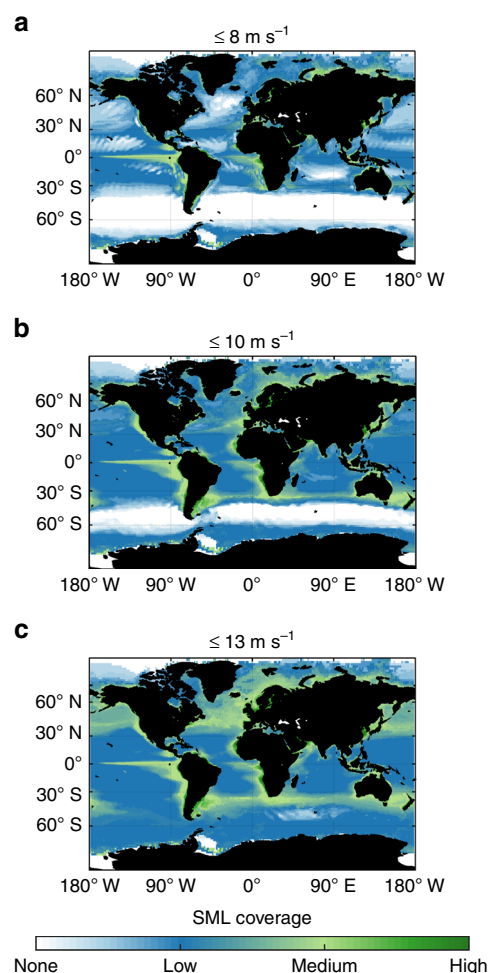


Fig. 1 Average annual sea surface microlayer coverage of the surface of the oceans. **a–c** Demonstrate the effect of different wind speed limits on the predicted global surface coverage. In particular, the North Atlantic and North Pacific as well as the Southern Ocean react rather sensitive to the chosen threshold values

concentration. In addition, we add a factor k_g to account for the impact of wind on the gas transfer velocities across the air–sea interface, which are largely determined by sea-surface roughness⁷. We keep μ_{photo} in units of $\text{mW s cm}^{-2} \text{day}^{-1}$ to allow for convenient conversion to daily VOC fluxes, as explained later. Here, we use averaged surfactant concentrations from field observations² and normalize μ_{photo} to the highest surfactant concentrations, commonly observed in eutrophic regions. $F_{\text{surfactant}}$ can therefore be expressed as

$$F_{\text{surfactant}} = \frac{\ln(c_{\text{surfactant}})}{\ln(c_{\text{max,surfactant}})} \quad (2)$$

with the surfactant concentration $c_{\text{surfactant}}$ (in concentration equivalents of Triton X), giving values between 0 and 1. For the gas transfer coefficient k_g , we apply the wind speed dependent parameterization of McGillis and co-workers²⁶ and normalize it to laboratory conditions of Ciuraru et al.¹⁰ and Brüggemann et al.¹⁴:

$$k_g = \frac{8.2 + 0.014 \cdot U_{10}^3}{8.2 + 0.014 \cdot U_{\text{lab}}^3} \quad (3)$$

with the wind speed U_{10} at 10 m height, and the sample flow speed under laboratory conditions $U_{\text{lab}} = 5.31 \times 10^{-2} \text{ m s}^{-1}$ (i.e., a flow rate of 200 mL min^{-1} scaled to a height of 10 m by assuming a log wind profile). Moreover, we perform all calculations at wind speed limits of 8, 10, and 13 m s^{-1} to account for the range of global SML abundances.

As shown in Fig. 2, μ_{photo} and, thus, photochemical VOC formation is expected to occur especially in coastal waters in the tropics throughout the entire year. However, in these regions elevated direct biological VOC emissions are also anticipated due to high microbiological activity in surface waters. Thus, total annual photochemical VOC emissions are of minor importance in such locations, despite constantly high values for μ_{photo} . Nonetheless, on shorter time scales interfacial photochemistry

might play a pivotal role here, e.g., during the decay of microalgae blooms. In contrast, for remote regions of the oceans with high solar radiation but lower biological activity, interfacial photochemistry can serve as a major source of VOCs over longer periods. The extent of this abiotic source for organic vapors typically varies with the season. For example, the southern Indian Ocean exhibits an elevated μ_{photo} for the seasons Jan–Mar and Oct–Dec, whereas the remote North Pacific shows similar photochemical potentials for the seasons Apr–Jun and Jul–Sep. We note that the extent and variability of μ_{photo} eventually depends on the SML formation dynamics, and thus also on the wind speed limit for SML formation. For example, the high values obtained for the Southern Ocean for the season of Oct–Dec rapidly decline to zero, if we set the wind speed limit for SML formation to 10 m s^{-1} (Supplementary Fig. 2). To predict μ_{photo} with higher time and space resolution, it is therefore essential to resolve the factors affecting SML coverage in more detail in future laboratory and field studies.

Up to now, field observations of photochemical VOC production from SMLs are scarce, which is certainly also due to the challenging differentiation between biologically and photochemically produced VOCs. However, Mungall et al. recently reported for the first time on interfacial photochemical production of oxygenated VOCs (OVOCs; e.g., formic acid, isocyanic acid, C₅-oxo acids, etc.) in the Arctic during July–August⁸. In general, the observed OVOCs exhibited a higher degree of oxidation compared to laboratory studies. However, this difference might simply be due to some initial oxidation reactions of the originally emitted VOCs in the atmosphere, as sampling occurred $\sim 15 \text{ m}$ above the sea surface. Moreover, the applied acetate chemical ionization mass spectrometer is in particular sensitive towards acidic compounds, such as the detected organic acids. In addition to such OVOC emissions, Burkart et al. found enhanced new particle formation in the Arctic summer at low wind speeds and sunny conditions⁹. However, since new particle formation is a complex process, we note that besides interfacial

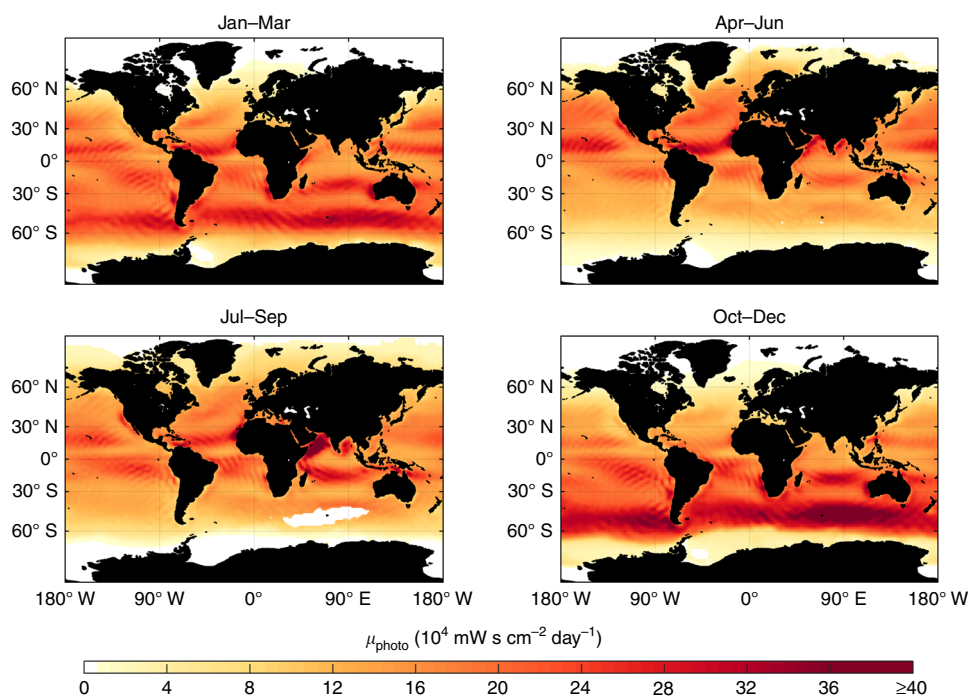


Fig. 2 Seasonal VOC emission potential from interfacial photochemistry of biogenic surfactants. The depicted estimations assume a sea surface microlayer wind speed limit of 13 m s^{-1} (for wind speed limits of 8 and 10 m s^{-1} , see Supplementary Figs. 1 and 2). Especially in remote marine regions with low microbiological activity, VOC formation from interfacial photochemistry is expected to play a significant role

photochemistry several other factors might have affected these observations significantly. Nevertheless, these field observations are in good agreement with our calculations, which show a maximum for μ_{photo} for the measurement location and time (indicated by the red circle in Fig. 3a and c). In contrast, Kim et al. found little to no evidence for isoprene formation from interfacial photochemistry for October–November in the same region²⁷. This observation is, nonetheless, again in good agreement with our predictions, giving a minimal μ_{photo} for this location and season (indicated by the red square in Fig. 3b and d). As a conservative estimate, i.e., an SML wind speed limit of 10 m s^{-1} (Fig. 3, panels a and b), we estimate an average μ_{photo} of $6.88 \times 10^4 \text{ mW s cm}^{-2} \text{ day}^{-1}$ and $1.30 \times 10^4 \text{ mW s cm}^{-2} \text{ day}^{-1}$ for the study periods and regions of Mungall et al.⁸ and Kim et al.²⁷, respectively. As can be seen from the figure, this large difference by a factor > 5 in μ_{photo} is mostly due to areas that are free of an SML under such conditions. The difference in μ_{photo} is, thus, decreasing when we allow the wind speed limit to increment to 13 m s^{-1} (Fig. 3, panels c and d). For these parameters the average μ_{photo} differs merely by a factor of about 1.2 for the two study periods and regions (i.e., 6.88×10^4 and 5.67×10^4 for Mungall et al.⁸ and Kim et al.²⁷, respectively). However, it is important to note that Kim et al.²⁷ observed high wind speeds of up to 25 m s^{-1} during their study period, with an average wind speed of 11 m s^{-1} . Formation and presence of prevalent SMLs, and hence, photochemical VOC formation at the air/sea interface, are unlikely under such conditions. Thus, our calculations for an ocean surface that is largely free of SMLs (i.e., Fig. 3b) is probably better reflecting the actual study period.

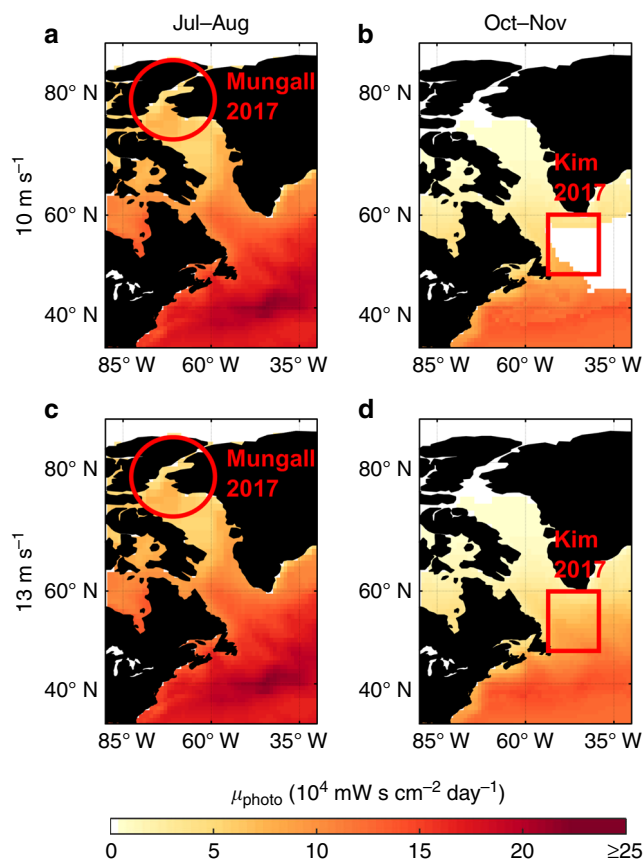


Fig. 3 VOC formation potential μ_{photo} . For wind speed limits of 10 m s^{-1} (a, b) and 13 m s^{-1} (c, d) for the locations and periods of the studies by Mungall et al.⁸ and Kim et al.²⁷, i.e., for Jul–Aug and Oct–Nov in the western North Atlantic and Arctic

Because of the demonstrated agreement between our predictions and these first field studies on interfacial photochemistry, we suggest utilizing μ_{photo} for future field campaigns to identify regions and time periods in which enhanced photochemical VOC production at the air/water interface can be expected. Moreover, to foster and support such studies in the ambient environment, we provide global distributions of μ_{photo} on a monthly basis for different SML wind speed limits (i.e., 8, 10, and 13 m s^{-1}) in the Supplementary Information (Supplementary Figs 1 and 2) and added the source code to an online repository (see “Code availability” section).

Marine isoprene emissions from interfacial photochemistry. A further benefit of μ_{photo} is that multiplication with VOC production values from laboratory experiments (in molecules $\text{mW}^{-1} \text{ s}^{-1}$) directly yields estimates on VOC emissions (in molecules $\text{cm}^{-2} \text{ day}^{-1}$). Thus, allowing us to approximate photochemical VOC emission fluxes for a certain region and season, even for single compounds. As a simple example, we estimate global annual isoprene emissions of 1.11 (0.70 – 1.52) Tg yr^{-1} from interfacial photochemistry (Fig. 4), using SML wind speed limits of 8 – 13 m s^{-1} and photochemical production values from recent laboratory observations for authentic SML samples^{10,11,14}. Emissions of other VOCs can easily be calculated in the same way. Comparison of this global flux to previously reported estimates on isoprene emissions demonstrates that interfacial photochemistry can compete, if not even surpass, direct biological emissions. Estimates from bottom-up studies, i.e., scaling up biological VOC emissions for different microorganism species, yield isoprene emissions in a similar range of 0.085 – 1.24 Tg yr^{-1} . However, it was also shown that top-down approaches, i.e., calculating isoprene fluxes by atmospheric chemistry models, suggest much larger isoprene emissions of 1.9 – 11.6 Tg yr^{-1} globally^{16,17,20,28,29}. Thus, accounting for interfacial photochemistry might aid in closing, or at least minimizing, this discrepancy between bottom-up and top-down approaches in global and regional models. In the same way, we infer total emissions of organic vapors from abiotic interfacial photochemistry in the range of 32.5 – 129 Tg C yr^{-1} (23.2 – 91.9 TgC yr^{-1}), hence, contributing significantly to marine VOC emissions.

We note that the approach presented here can solely give an estimate on average monthly VOC fluxes from interfacial photochemistry. Thus, more sophisticated models with higher time and space resolution will be necessary, to predict photochemical VOC fluxes on a daily or even hourly basis. Nonetheless, as shown in Table 1, a direct comparison of observed and

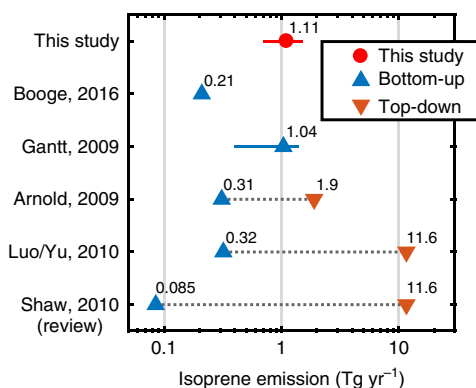


Fig. 4 Comparison of current global isoprene emission estimates and the results of our study (0.70 – 1.52 Tg yr^{-1}). The bottom-up estimates are based on direct biological emissions only, whereas top-down refers to expected total isoprene emissions from global model calculations

Table 1 Comparison of observed and calculated isoprene fluxes for single field studies

Field study	Comment	Location	Latitude ^a	Longitude	Period	Observed flux ^b 10 ¹² molecules cm ⁻² day ⁻¹	Calculated flux
Hackenberg et al. ⁴¹	AMT22 AMT23	Atlantic	60° N–50° S	30° W	Oct–Nov	5.27 ± 3.97 (0.11–19.9) 3.80 ± 4.23 (0.0043–29.4)	4.18–11.1
	ACCACIA1 ACCACIA2	North Atlantic/Arctic	70–77° N	15° W–15° E	Mar	0.59 ± 0.78 (0.035–4.32)	0.00–2.04
Kim et al. ²⁷		North Atlantic	55–60° N	44–54° W	Jul–Aug	2.59 ± 2.68 (0.026–12.1)	3.40–5.67
Tran et al. ⁴²		North Atlantic	55–60° N	44–54° W	Oct–Nov	4.32 ± 16.4	0.00–3.48
	Wan L&M	North Atlantic (Atl. water)	60–80° N	15° W–15° E	Jun–Jul	8.91 ± 23.4 5.12 ± 12.3	4.56–7.60
	Wan L&M	Arctic (polar water)				2.53 ± 2.17 1.45 ± 1.20	
Meskhidze and Nenes ^{d,43}	SOFeX Palmer/Shaw	Southern Ocean	40–60° S	20–55° W	Annual	5.18 (0.86–19.01) 15.55 (1.73–74.30)	0.10–10.4
Broadgate et al. ⁴⁴		North Sea	57° N	3° W	Annual	1.47 (0.09–4.06)	3.18–5.89
Milne et al. ⁴⁵		Florida Gulf	24° N	81° W	Sept	2.94 (0.57–6.05)	5.72–9.55
Baker et al. ⁴⁶		Eastern North Atlantic	53° N	13° W	May	2.94 (1.04–7.69)	0.00–12.1
Matsunaga et al. ⁴⁷		North Pacific	35° N	147° E	May	1.90–18.14	0.00–13.7
Sinha et al. ⁴⁸	Mesocosm experiment	North Sea	60° N	5° E	May–Jun	58.75 ± 11.08	4.82–8.05

^a Latitude and longitude area used for flux calculation
^b flux mean ± standard deviation (range)
^c Wan = flux parametrization from Wanninkhof⁴⁹, L&M = flux parametrization from Liss and Merlivat⁵⁰
^d remotely sensed data, see original reference for method description

calculated isoprene fluxes demonstrates already a good agreement for single field studies, typically predicting somewhat lower fluxes than the reported ones. Remarkably, for almost all studies even the maximum predicted values do not exceed the range of observed isoprene emission fluxes. This general underprediction of isoprene emission fluxes compared to field studies is consistent with the assumption that interfacial photochemistry represents an additional VOC source besides direct biological emissions, significantly contributing to total marine VOC fluxes.

In particular, photochemical production and emission of larger (unsaturated) VOCs, such as isoprene, seems important, since few other abiotic formation pathways are known for such compounds in the marine environment. In contrast, the contribution to fluxes of smaller VOCs, such as acetone, or acetaldehyde, is probably less significant, since a large variety of strong sources exists in both the atmosphere and the ocean. As an example, Yang et al.³⁰ observed emission fluxes of acetone and acetaldehyde of 7.11×10^{14} and 3.9×10^{14} molecules cm⁻² day⁻¹, respectively, during a cruise in the tropical Atlantic (3–39° N). However, our calculations merely predict emission fluxes in the range of $0.58\text{--}1.1 \times 10^{14}$ and $0.20\text{--}0.60 \times 10^{14}$ molecules cm⁻² day⁻¹ from interfacial photochemistry for acetone and acetaldehyde, respectively.

Implications for marine organic aerosol mass. To assess possible implications of this yet unaccounted VOC source on OA mass loadings in the marine boundary layer, we calculate the formation of secondary OA (SOA) from unsaturated VOC oxidation products. To approximate background aerosol concentrations, primary OA emissions are estimated based on biological activity and surface wind speeds^{17,18,31} (Supplementary Fig. 3). As depicted in Fig. 5, our results indicate that especially in tropical regions with low POA concentrations additional SOA from oxidation of photochemically produced VOCs is important, contributing up to 60% of additional OA mass (e.g., in the Indian

Ocean during Oct–Dec). Moreover, our calculations show a reasonable agreement with field studies in such remote regions (Supplementary Table 1). As an example, we obtain similar trends for OA mass concentrations as reported from long term observations on Amsterdam Island (37.8° S, 77.6° E; Supplementary Fig. 4)³². As already seen for the calculation of VOC fluxes, we typically observe a certain underprediction of total OA mass concentrations. This is, however, supporting again the hypothesis that SOA from photochemically produced VOCs is adding up on biologically derived SOA mass, which we omit in our calculations. In total, we estimate the additional annual SOA mass due to interfacial photochemistry to be in the range of 0.48–0.60 Tg yr⁻¹. Oxidation products of photochemically produced isoprene are expected to contribute 33–73 Gg yr⁻¹ to this total SOA mass, corresponding to about 0.2–0.5% of marine OA mass, which is in agreement with recent field observations^{33,34}. Nonetheless, our estimations probably represent a lower limit, since we do not account for additional oxidation pathways of the formed VOCs, e.g., via ozone chemistry. In addition, we assume instantaneous mixing of the emitted VOCs into the entire volume of the MBL, probably leading to a rather diluted scenario compared to ambient conditions.

Despite remaining uncertainties, our study demonstrates that abiotic VOC production from interfacial photochemistry might serve as a major contributor to marine VOC levels and OA mass loadings. Isoprene emissions from photochemistry are expected to be in the same range as direct biological emissions and might even dominate depending on location and season. Moreover, SOA formation from oxidation of photochemically produced VOCs might explain field observations of new particle formation events which are occurring decoupled from biological activity. Therefore, we suggest that VOC and SOA production from interfacial photochemistry should be taken into account to accurately model and predict atmospheric chemistry and related processes, such as ozone cycling and cloud formation.

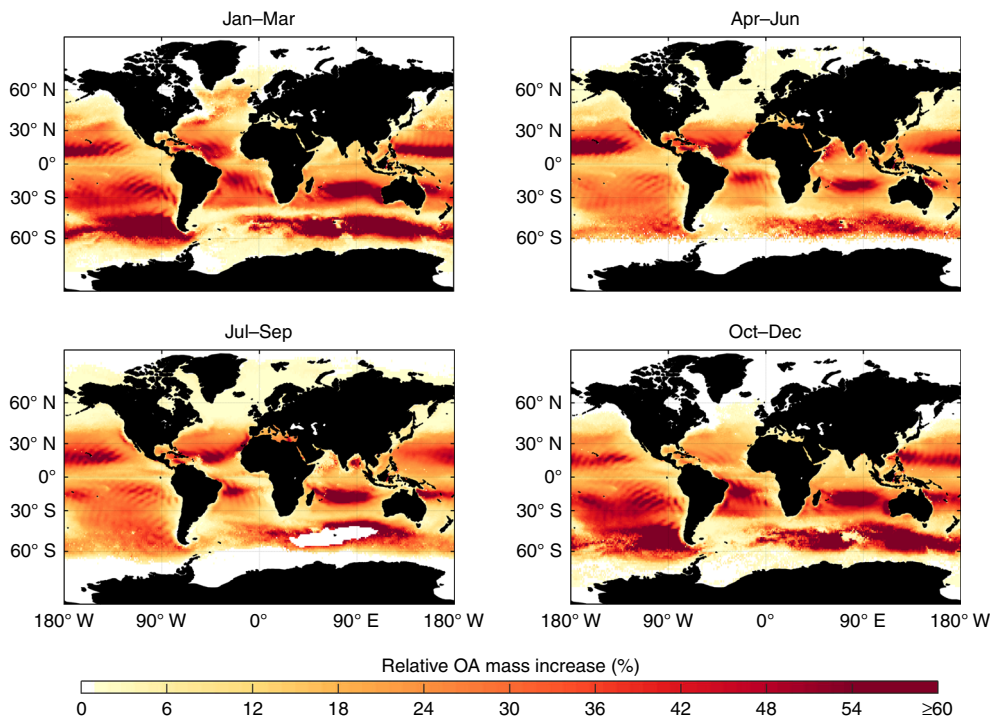


Fig. 5 Seasonal estimates on the organic aerosol mass contribution in the marine boundary layer from oxidation of photochemically produced VOCs for an SML wind speed limit of 13 m s^{-1} . For wind speed limits of 8 and 10 m s^{-1} , see Supplementary Figs 5 and 6. Here, only OH oxidation of unsaturated volatile organic compounds was taken into account, assuming similar secondary organic aerosol yields as given by Tsimpidi et al.²³

Methods

Software and data processing. All data processing was conducted using Matlab (version 8.6, R2015b, Mathworks Inc.), including the `m_map` tools package (v1.4h, <https://www.eoas.ubc.ca/~rich/map.html>) for the production of global maps. A general overview on all data sources and calculations is given in Supplementary Fig. 7. Moreover, the Matlab code as well as a stand-alone version of the Photochemistry At Liquid/Air interfaces containing Surfactants (PhotochemATLAS) model, including instructions, is publicly available on Bitbucket, an online community repository.

Production of organic vapors from interfacial photochemistry. For all calculations on photochemical VOC production presented here, we used the following three major assumptions. First, for the total surface area that is available for photochemistry, the air/water interface of the ocean is treated as a flat surface. We note that this simplification might eventually lead to an underestimation of VOC production, since it neglects increases in surface area, e.g., from waves, at the ocean's surface. Nonetheless, since sea surface roughness is known to enhance gas diffusivity of the ocean's air/water interface⁷, we estimate air-sea gas transfer velocities of VOCs as a function of wind speed, using the empirical parameterization of McGillis et al.²⁶. In contrast to other common parameterization, this cubic $k-U_{10}$ relationship is predicting non-zero emissions at zero wind speed, which is in agreement with laboratory studies on interfacial photochemistry and VOC production^{10,11,14}. As shown in Supplementary Fig. 8, the wind speed-dependent gas transfer velocities can increase the calculated VOC fluxes by up to a factor of ~ 4.7 (i.e., in the Southern Ocean) compared to assuming constant gas transfer velocities across the air/sea interface. However, we note that there remains significant uncertainty of at least a factor of two in transfer velocities, as it is commonly the case for all trace gas emissions from the ocean into the atmosphere up to now^{35,36}.

Second, photochemical VOC production correlates linearly with solar radiation, whereas a logarithmic decay with decreasing surfactant concentrations is observed^{10,11}. This assumption is corroborated by measurements of Rossignol et al.¹², who reported that absorbance at a specific wavelength is a linear function of the surfactant concentration. Moreover, Ciuraru et al.^{10,11} demonstrated that VOC production follows a logarithmic decay with decreasing surfactant concentrations. In addition, these assumptions are also consistent with the hypothesis that especially photosensitized reactions are driving VOC production from interfacial photochemistry³⁷. Nonetheless, we note that these laboratory studies use single compounds as surfactants, whereas the ambient SML is a highly complex and dynamically changing composition of organic and inorganic compounds. Thus, we cannot exclude deviations for specific SML samples from these simplified assumptions.

Third, only radiation in the wavelength region of 280–400 nm initiates photochemical production of VOCs, since shorter wavelength might lead to photolysis, whereas the energy of longer wavelength is not sufficient to induce photochemical reactions. Furthermore, laboratory observations commonly used this wavelength range to infer photochemical production and fluxes of VOC^{10–14}.

Given these constraints, we calculated a daily photochemical VOC emission potential μ_{photo} (in $\text{mW s cm}^{-2} \text{ day}^{-1}$) for the air/water interface of each 1-by-1 degree grid cell (Eq. (1)) with the length of the day t_{sun} (in s), solar radiation UV_{ab} at the Earth's surface (in $\text{mW cm}^{-2} \text{ day}^{-1}$), and a unitless correction factor $F_{\text{surfactant}}$ to account for SML coverage and surfactant concentration (Eq. (2)). Moreover, we accounted for changes in gas transfer velocities across the air/sea interface by applying the wind speed-dependent factor k_g , which we normalize to laboratory conditions (Eq. (3)). As explained further below, we keep μ_{photo} in units of $\text{mW s cm}^{-2} \text{ day}^{-1}$ to allow for convenient conversion to daily VOC fluxes.

As depicted in Supplementary Fig. 7, for t_{sun} and UV_{ab} we used climatological data on solar irradiation at the surface of the Earth in the UV-a (315–400 nm) and UV-b (280–315 nm) range from the NCAR TUV model (<https://www2.acom.ucar.edu/modeling/tropospheric-ultraviolet-and-visible-tuv-radiation-model>), giving monthly averaged UV irradiance values (i.e., considering ozone, cloudiness, and t_{sun}) for the period of 1979–2000. The data was refined from $1^\circ \times 1.25^\circ$ resolution to $1^\circ \times 1^\circ$ resolution by linear interpolation for all further calculations.

Global mapping of the ocean's surfactant concentrations ($c_{\text{surfactant}}$) and SML coverage was conducted according to the method described by Wurl et al.². First, oligo-, meso- and eutrophic regions of the ocean were identified from global maps of net primary production (NPP), based on the Vertically Generalized Production Model³⁸. Monthly data on NPP were obtained from the ocean productivity webpage of the Oregon State University (<http://www.science.oregonstate.edu/ocean.productivity>), ranging from July 2002 to November 2016 (Supplementary Fig. 9). After averaging the data for each month and lowering the resolution from $0.17^\circ \times 0.17^\circ$ to $1^\circ \times 1^\circ$ by linear interpolation, trophic states were defined as follows: oligotrophic waters with $\text{NPP} < 0.4 \text{ g C m}^{-2} \text{ day}^{-1}$, mesotrophic waters with NPP between 0.4 and $1.2 \text{ g C m}^{-2} \text{ day}^{-1}$, and eutrophic waters with $\text{NPP} > 1.2 \text{ g C m}^{-2} \text{ day}^{-1}$. Then, average surfactant concentrations were assigned to trophic states, based on mean values of Triton X equivalents ($\mu\text{g Teq L}^{-1}$) from field observations². The assigned surfactant concentrations are as follows: for oligotrophic waters $c_{\text{surfactant}} = 320 \mu\text{g Teq L}^{-1}$ (i.e., low SML coverage), for mesotrophic waters $c_{\text{surfactant}} = 502 \mu\text{g Teq L}^{-1}$ (i.e., medium SML coverage), and for eutrophic waters $c_{\text{surfactant}} = 663 \mu\text{g Teq L}^{-1}$ (i.e., high SML coverage).

Furthermore, SML coverage was estimated for upper wind speed limits of 8, 10, and 13 m s^{-1} . These values were reported earlier as maximum surface wind speed for SML formation^{2,24,25}. Data on monthly mean surface wind speeds (January 1946–June 2016) were obtained from NCEP/NCAR reanalysis project (<http://www.esrl.noaa.gov>) and averaged for each month (Supplementary Fig. 10). Then, the monthly data were refined from $2.5^\circ \times 2.5^\circ$ resolution to $1^\circ \times 1^\circ$ resolution by linear

interpolation. All regions exceeding the selected wind speed limit were considered as free of SMLs and, thus, considered as photochemically not active.

For our estimations, we normalized μ_{photo} to the highest surfactant concentrations $c_{\text{max, surfactant}}$ as observed in eutrophic regions (i.e., $663 \mu\text{g Teq L}^{-1}$). Furthermore, we assumed photochemical VOC production to exhibit a logarithmic decay with decreasing surfactant concentrations^{10,11}. $F_{\text{surfactant}}$ was therefore expressed as shown in Eq. (2).

The effect of this correction factor on photochemical VOC production is illustrated in Supplementary Fig. 11, demonstrating reduced VOC production at lower surfactant concentrations^{10,11}. For the lowest surfactant concentration of $320 \mu\text{g Teq L}^{-1}$, commonly observed in oligotrophic regions², $F_{\text{surfactant}}$ will reduce the estimated photochemical VOC emissions by ca. 11%. For mesotrophic conditions, i.e., $c_{\text{surfactant}} = 502 \mu\text{g Teq L}^{-1}$, a reduction of about 4% is expected. We stress that up to now this correction is solely based on laboratory studies for single compounds, whereas the ambient SML is a complex mixture of organic and inorganic compounds. Therefore, we suggest focusing in future studies on more complex mixtures of surfactants, ambient SML samples, and also the relationship between surface pressure and VOC production.

To infer estimates on photochemical VOC production and emission of single compounds from interfacial photochemistry at the surface of the ocean, μ_{photo} is multiplied by data from VOC flux measurements in laboratory studies:

$$\text{VOC}_{\text{ambient}} = \text{VOC}_{\text{lab}} \cdot \mu_{\text{photo}} \quad (4)$$

with the estimated VOC emissions $\text{VOC}_{\text{ambient}}$ (in molecules $\text{cm}^{-2} \text{day}^{-1}$), measured photochemical VOC emissions from laboratory studies VOC_{lab} (in molecules $\text{mW}^{-1} \text{s}^{-1}$), and the photochemical potential μ_{photo} . Values for VOC_{lab} can readily be obtained from photochemical experiments under controlled conditions, using common VOC measurement techniques such as proton transfer reaction mass spectrometry (PTR-MS). In this study we used such data from previous work of George and co-workers^{10,11,14}. For example, to estimate global emissions of isoprene from interfacial photochemistry, we used previously reported values for VOC_{lab} from marine SML and biofilm samples^{10,11,14}, which are in the range of $3.71\text{--}6.19 \times 10^7$ molecules $\text{mW}^{-1} \text{s}^{-1}$.

Estimating secondary organic aerosol formation. As depicted in Supplementary Fig. 7, the VOC module described above is coupled to an SOA module, which we utilized to retrieve estimates on potential SOA formation from photochemically produced and emitted VOCs. This module is based on equilibrium partitioning theory²¹ and a one-dimensional volatility basis set²², lumping VOC oxidation products in 10 volatility bins with saturation vapor pressures of $\log C^*(300 \text{ K}) = \{-3, -2, -1, 0, 1, 2, 3, 4, 5, 6\} \mu\text{g m}^{-3}$. Since so far no parameterization of SOA yields for oxidation of VOCs from interfacial photochemistry is available, here we accounted solely for oxidation of unsaturated VOCs by OH radicals, using SOA yields for alkenes previously given by Tsimpidi et al.²³ (i.e., OLE2-case at low NO_x concentrations; $\alpha = \{0, 0, 0, 0.023, 0.044, 0.129, 0.375, 0, 0, 0\}$). Moreover, we assumed pseudo-first order kinetics for the reaction of VOCs with OH radicals. We attempted to approximate the reaction rate constant k_{OH} for the mixture of unsaturated VOCs by averaging known k_{OH} constants of similar compounds³⁹. An overview of the compounds and rate constants used for this approximation is given in Supplementary Table 2. Using these values we found a mean reaction rate constant of $k_{\text{OH}} = 109.76 \times 10^{12} \text{ cm}^3 \text{ molecule}^{-1} \text{ s}^{-1}$, which was then applied to estimate formation of VOC oxidation products. For all calculations, we used an OH concentration of $c_{\text{OH}} = 1.5 \times 10^6$ molecules cm^{-3} . Unless stated otherwise, the aging time for SOA formation and growth was set to 12 h per day at a temperature of 15 °C.

In addition, we estimated primary organic aerosol (POA) mass fluxes and concentrations above the ocean, in order to model accurately the partitioning of VOC oxidation products. POA was, however, solely regarded as background aerosol, which was not taking part in partitioning, i.e., POA was defined as non-volatile. Here we applied established POA emission schemes, which infer POA fluxes from sea surface temperature, chlorophyll-a concentration, and surface wind speed^{18,39}. Monthly mean data on sea surface temperature and chlorophyll-a concentrations were obtained from MODIS ocean products (<https://modis.gsfc.nasa.gov/>). POA emissions were instantaneously diluted into the marine boundary layer (MBL). Monthly mean MBL heights were obtained from the NOAA-CIRES 20th Century Reanalysis project (https://www.esrl.noaa.gov/psd/data/20thC_Rean/) (Supplementary Fig. 12).

As a simplified example, Supplementary Fig. 13 shows the result of a simulation of VOC formation and oxidation, as well as SOA particle formation for one grid cell. In this case, the following parameters were used: a POA mass concentration of $0.4 \mu\text{g m}^{-3}$ (i.e., representing typical remote marine air⁴⁰), an ambient temperature of 20 °C, an MBL height of 600 m, and an emission rate of unsaturated VOCs of $\text{VOC}_{\text{ambient}} = 4.1 \times 10^9$ molecules $\text{cm}^{-2} \text{s}^{-1}$ (i.e., representing tropical regions). Both VOC formation from interfacial photochemistry and oxidation of the gas-phase products start at time 0. The resulting mixing ratio of, yet unreacted, unsaturated VOCs is depicted in the left panel of the figure, reaching a steady state of ca. 4×10^8 molecules cm^{-3} (i.e., 16 pptv) after 8 h. This equilibrium mixing ratio might seem quite low, however, we note that here we assume instantaneous mixing of the emitted VOCs into the entire volume of the MBL. Therefore, ambient mixing ratios in direct proximity of the air/water interface (i.e., a few meters above the surface of

the ocean) are likely to be much larger, whereas our calculations solely represent a lower limit.

Nonetheless, even for this dilute scenario we observe significant SOA formation from VOC oxidation products, as depicted in the right panel of Supplementary Fig. 13. Despite direct formation of VOC oxidation products, for the first 2 h almost no increase in OA mass concentration is observed. This delayed increase in particle mass is due to the enhanced partitioning of oxidation products to the gas phase until a critical gas-phase concentration is reached. After this initial period, low volatile oxidation products start to partition into the particle phase, resulting in an increase in OA particle mass concentration. This increase is then accelerating with ongoing formation of VOC oxidation products. In this simplified example, eventually a total increase of $0.088 \mu\text{g m}^{-3}$ is observed after a total aging time of 12 h, i.e., a relative increase of 22% in OA particle mass. Again, this value represents solely a lower limit of enhanced SOA formation, since we excluded ozone chemistry, which would generate additional low volatility oxidation products, probably enhancing OA particle mass concentrations.

Code availability. The Matlab code of the Photochemistry At Liquid/Air interfaces containing Surfactants (PhotochemATLAS) model, including instructions, is publicly available on the online community repository Bitbucket (https://bitbucket.org/bruggemann_m/photochematlas).

Data availability. Further data sets generated during this study are available from the corresponding author upon reasonable request.

Received: 6 September 2017 Accepted: 23 April 2018

Published online: 29 May 2018

References

- George, C., Ammann, M., D'Anna, B., Donaldson, D. J. & Nizkorodov, S. A. Heterogeneous photochemistry in the atmosphere. *Chem. Rev.* **115**, 4218–4258 (2015).
- Wurl, O., Wurl, E., Miller, L., Johnson, K. & Vagle, S. Formation and global distribution of sea-surface microlayers. *Biogeosciences* **8**, 121–135 (2011).
- Wurl, O., Stolle, C., Van Thuoc, C., The Thu, P. & Mari, X. Biofilm-like properties of the sea surface and predicted effects on air-sea CO₂ exchange. *Prog. Oceanogr.* **144**, 15–24 (2016).
- Cunliffe, M. et al. Sea surface microlayers: a unified physicochemical and biological perspective of the air–ocean interface. *Prog. Oceanogr.* **109**, 104–116 (2013).
- Engel, A. et al. The ocean's vital skin: toward an integrated understanding of the sea surface microlayer. *Front. Mar. Sci.* **4**, 165 (2017).
- Van Pinxteren, M. et al. The influence of environmental drivers on the enrichment of organic carbon in the sea surface microlayer and in submicron aerosol particles – measurements from the Atlantic Ocean. *Elem. Sci. Anth.* **5**, 35 (2017).
- Wurl, O., Ekau, W., Landing, W. M. & Zappa, C. J. Sea surface microlayer in a changing ocean – a perspective. *Elem. Sci. Anth.* **5**, 31 (2017).
- Mungall, E. L. et al. Microlayer source of oxygenated volatile organic compounds in the summertime marine Arctic boundary layer. *Proc. Natl Acad. Sci. USA* **114**, 6203–6208 (2017).
- Burkart, J. et al. Summertime observations of elevated levels of ultrafine particles in the high Arctic marine boundary layer. *Atmos. Chem. Phys.* **17**, 5515–5535 (2017).
- Ciuraru, R. et al. Photosensitized production of functionalized and unsaturated organic compounds at the air-sea interface. *Sci. Rep.* **5**, 12741 (2015).
- Ciuraru, R. et al. Unravelling new processes at interfaces: photochemical isoprene production at the sea surface. *Environ. Sci. Technol.* **49**, 13199–13205 (2015).
- Rosignol, S. et al. Atmospheric photochemistry at a fatty acid-coated air-water interface. *Science* **353**, 699–702 (2016).
- Bernard, F., Ciuraru, R., Boréave, A. & George, C. Photosensitized formation of secondary organic aerosols above the air/water interface. *Environ. Sci. Technol.* **50**, 8678–8686 (2016).
- Brüggemann, M. et al. Interfacial photochemistry of biogenic surfactants: a major source of abiotic volatile organic compounds. *Faraday Discuss.* **352**, 357–363 (2017).
- Alpert, P. A. et al. Fatty acid surfactant photochemistry results in new particle formation. *Sci. Rep.* **7**, 12693 (2017).
- Arnold, S. R. et al. Evaluation of the global oceanic isoprene source and its impacts on marine organic carbon aerosol. *Atmos. Chem. Phys.* **9**, 1253–1262 (2009).

17. Gantt, B., Meskhidze, N. & Kamykowski, D. A new physically-based quantification of marine isoprene and primary organic aerosol emissions. *Atmos. Chem. Phys.* **9**, 4915–4927 (2009).
18. Gantt, B. et al. Model evaluation of marine primary organic aerosol emission schemes. *Atmos. Chem. Phys.* **12**, 8553–8566 (2012).
19. Gantt, B., Glotfelty, T., Meskhidze, N. & Zhang, Y. Simulating the impacts of marine organic emissions on global atmospheric chemistry and aerosols using an online-coupled meteorology and chemistry model. *Atmos. Clim. Sci.* **5**, 266–274 (2015).
20. Shaw, S. L., Gantt, B. & Meskhidze, N. Production and emissions of marine isoprene and monoterpenes: a review. *Adv. Meteorol.* **2010**, 1–24 (2010).
21. Odum, J. A. Y. R. et al. Gas/particle partitioning and secondary organic aerosol yields. *Environ. Sci. Technol.* **30**, 2580–2585 (1996).
22. Donahue, N. M., Robinson, A. L., Stanier, C. O. & Pandis, S. N. Coupled partitioning, dilution, and chemical aging of semivolatile organics. *Environ. Sci. Technol.* **40**, 2635–2643 (2006).
23. Tsimpidi, A. P. et al. Evaluation of the volatility basis-set approach for the simulation of organic aerosol formation in the Mexico City metropolitan area. *Atmos. Chem. Phys.* **10**, 525–546 (2010).
24. Gantt, B. et al. Wind speed dependent size-resolved parameterization for the organic mass fraction of sea spray aerosol. *Atmos. Chem. Phys.* **11**, 8777–8790 (2011).
25. Sabbaghzadeh, B., Upstill-Goddard, R. C., Beale, R., Pereira, R. & Nightingale, P. D. The Atlantic Ocean surface microlayer from 50° N to 50° S is ubiquitously enriched in surfactants at wind speeds up to 13 m s⁻¹. *Geophys. Res. Lett.* **44**, 2852–2858 (2017).
26. McGillis, W. R. et al. Air-sea CO₂ exchange in the equatorial Pacific. *J. Geophys. Res. Oceans* **109**, C08S2 (2004).
27. Kim, M. J. et al. Air-Sea exchange of biogenic volatile organic compounds and the impact on aerosol particle size distributions. *Geophys. Res. Lett.* **44**, 3887–3896 (2017).
28. Booge, D. et al. Can simple models predict large-scale surface ocean isoprene concentrations? *Atmos. Chem. Phys.* **16**, 11807–11821 (2016).
29. Luo, G. & Yu, F. A numerical evaluation of global oceanic emissions of α -pinene and isoprene. *Atmos. Chem. Phys.* **10**, 2007–2015 (2010).
30. Yang, M. et al. Air-sea fluxes of oxygenated volatile organic compounds across the Atlantic Ocean. *Atmos. Chem. Phys.* **14**, 7499–7517 (2014).
31. Lana, A., Simó, R., Vallina, S. M. & Dachs, J. Potential for a biogenic influence on cloud microphysics over the ocean: a correlation study with satellite-derived data. *Atmos. Chem. Phys.* **12**, 7977–7993 (2012).
32. Sciare, J. et al. Long-term observations of carbonaceous aerosols in the Austral Ocean atmosphere: evidence of a biogenic marine organic source. *J. Geophys. Res.* **114**, D15302 (2009).
33. Fu, P., Kawamura, K. & Miura, K. Molecular characterization of marine organic aerosols collected during a round-the-world cruise. *J. Geophys. Res.* **116**, D13302 (2011).
34. Hu, Q.-H. et al. Secondary organic aerosols over oceans via oxidation of isoprene and monoterpenes from Arctic to Antarctic. *Sci. Rep.* **3**, 2280 (2013).
35. Lana, A. et al. An updated climatology of surface dimethylsulfide concentrations and emission fluxes in the global ocean. *Glob. Biogeochem. Cycles* **25**, GB1004 (2011).
36. Johnson, M. T. A numerical scheme to calculate temperature and salinity dependent air-water transfer velocities for any gas. *Ocean Sci.* **6**, 913–932 (2010).
37. Tinel, L. et al. Mechanistic insights on the photosensitized chemistry of a fatty acid at the air/water interface. *Environ. Sci. Technol.* **50**, 11041–11048 (2016).
38. Behrenfeld, M. J. & Falkowski, P. G. Photosynthetic rates derived from satellite-based chlorophyll concentration. *Limnol. Oceanogr.* **42**, 1–20 (1997).
39. Atkinson, R. & Arey, J. Atmospheric degradation of volatile organic compounds. *Chem. Rev.* **103**, 4605–4638 (2003).
40. Meskhidze, N. et al. Production mechanisms, number concentration, size distribution, chemical composition, and optical properties of sea spray aerosols. *Atmos. Sci. Lett.* **14**, 207–213 (2013).
41. Hackenberg, S. C. et al. Potential controls of isoprene in the surface ocean. *Glob. Biogeochem. Cycles* **31**, 644–662 (2017).
42. Tran, S. et al. A survey of carbon monoxide and non-methane hydrocarbons in the Arctic Ocean during summer 2010. *Biogeosciences* **10**, 1909–1935 (2013).
43. Meskhidze, N. & Nenes, A. Phytoplankton and cloudiness in the Southern. *Ocean Sci.* **314**, 1419–1423 (2006).
44. Broadgate, W. J., Liss, P. S. & Penkett, S. A. Seasonal emissions of isoprene and other reactive hydrocarbon gases from the ocean. *Geophys. Res. Lett.* **24**, 2675–2678 (1997).
45. Milne, P. J., Riemer, D. D., Zika, R. G. & Brand, L. E. Measurement of vertical distribution of isoprene in surface seawater, its chemical fate, and its emission from several phytoplankton monocultures. *Mar. Chem.* **48**, 237–244 (1995).
46. Baker, A. R. et al. Distribution and sea-air fluxes of biogenic trace gases in the eastern Atlantic Ocean. *Glob. Biogeochem. Cycles* **14**, 871–886 (2000).
47. Matsunaga, S., Mochida, M., Saito, T. & Kawamura, K. In situ measurement of isoprene in the marine air and surface seawater from the western North Pacific. *Atmos. Environ.* **36**, 6051–6057 (2002).
48. Sinha, V. et al. Air-sea fluxes of methanol, acetone, acetaldehyde, isoprene and DMS from a Norwegian fjord following a phytoplankton bloom in a mesocosm experiment. *Atmos. Chem. Phys.* **7**, 739–755 (2007).
49. Wanninkhof, R. Relationship between wind speed and gas exchange over the ocean. *J. Geophys. Res.* **97**, 7373–7382 (1992).
50. Liss, P. S. & Merlivat, L. in *The Role of Air-Sea Exchange in Geochemical Cycling*. NATO ASI Series (Series C: Mathematical and Physical Sciences), vol. 185 (ed. Buat-Ménard, P.) 113–127 (Springer, Dordrecht, 1986).

Acknowledgements

This study was supported by the European Research Council under the European Union's Framework Program (FP/2007-2013)/ERC Grant Agreement 290852—AIRSEA. This project has also received funding from the European Union's Horizon 2020 research and innovation program under grant agreement No. 730997 (EUROCHAMP2020) and 690958 (MARSU). We thank S. Madronich and the NCAR for providing UV irradiation climatologies from the TUV model. We acknowledge the Physical Sciences Division of NOAA/ESRL for providing data on monthly wind speeds and MBL heights.

Author contributions

M.B. scripted the code, performed the calculations, and wrote the paper. All authors designed the study. C.G. supervised the project. All authors contributed comments to the manuscript.

Additional information

Supplementary Information accompanies this paper at <https://doi.org/10.1038/s41467-018-04528-7>.

Competing interests: The authors declare no competing interests.

Reprints and permission information is available online at <http://npg.nature.com/reprintsandpermissions/>

Publisher's note: Springer Nature remains neutral with regard to jurisdictional claims in published maps and institutional affiliations.



Open Access This article is licensed under a Creative Commons Attribution 4.0 International License, which permits use, sharing, adaptation, distribution and reproduction in any medium or format, as long as you give appropriate credit to the original author(s) and the source, provide a link to the Creative Commons license, and indicate if changes were made. The images or other third party material in this article are included in the article's Creative Commons license, unless indicated otherwise in a credit line to the material. If material is not included in the article's Creative Commons license and your intended use is not permitted by statutory regulation or exceeds the permitted use, you will need to obtain permission directly from the copyright holder. To view a copy of this license, visit <http://creativecommons.org/licenses/by/4.0/>.

© The Author(s) 2018